# Trypanosoma brucei FKBP12 differentially controls motility and cytokinesis in procyclic and bloodstream forms.

Anaïs Brasseur, Brice Rotureau, Marjorie Vermeersch, Thierry Blisnick, Didier Salmon, Philippe Bastin, Etienne Pays, Luc Vanhamme, David Pérez-Morga

EC
Journals.ASM.org

# *Trypanosoma brucei* FKBP12 Differentially Controls Motility and Cytokinesis in Procyclic and Bloodstream Forms

**Anaïs Brasseur,[a,b] Brice Rotureau,[c] Marjorie Vermeersch,[d] Thierry Blisnick,[c] Didier Salmon,[e] Philippe Bastin,[c] Etienne Pays,[a] Luc Vanhamme,[a] David Pérez-Morga[a,d]**

Laboratory of Molecular Parasitology, IBMM, Université Libre de Bruxelles, Gosselies, Belgium[a]; Molecular and Cellular Parasitology, Department of Biological Sciences, National University of Singapore, Singapore, Singapore[b]; Trypanosome Cell Biology Unit, CNRS URA 2581 and Parasitology Department, Pasteur Institute, Paris, France[c]; Center for Microscopy and Molecular Imaging–CMMI Université Libre de Bruxelles, Gosselies, Belgium[d]; Institute of Medical Biochemistry, Centro de Ciências e da Saude, Federal University of Rio de Janeiro, Rio de Janeiro, Brazil[e]

**FKBP12 proteins are able to inhibit TOR kinases or calcineurin phosphatases upon binding of rapamycin or FK506 drugs, respectively. The *Trypanosoma brucei* FKBP12 homologue (TbFKBP12) was found to be a cytoskeleton-associated protein with specific localization in the flagellar pocket area of the bloodstream form. In the insect procyclic form, RNA interference-mediated knockdown of *TbFKBP12* affected motility. In bloodstream cells, depletion of TbFKBP12 affected cytokinesis and cytoskeleton architecture. These last effects were associated with the presence of internal translucent cavities limited by an inside-out configuration of the normal cell surface, with a luminal variant surface glycoprotein coat lined up by microtubules. These cavities, which recreated the streamlined shape of the normal trypanosome cytoskeleton, might represent unsuccessful attempts for cell abscission. We propose that TbFKBP12 differentially affects stage-specific processes through association with the cytoskeleton.**

African trypanosomes are extracellular protozoan flagellated parasites responsible for sleeping sickness in humans and nagana in cattle. The life cycle of *Trypanosoma brucei* encompasses different stages, including the long slender bloodstream forms (BF) proliferating in mammalian blood and the procyclic forms (PF) that actively multiply in the gut of the *Glossina* vector (1).

Trypanosomes are among the most divergent eukaryotes in evolution and display specific features, many of which are related to cell division probably due to the fact that most organelles are present at one copy per cell and have to be duplicated and segregated synchronously between the daughter cells. This division involves check points that differ from those of other eukaryotes, such as the control of karyokinesis when cytokinesis is inhibited (2, 3) and vice versa (4). Molecular effectors of these check points, such as mitogen-activated protein kinase and cyclin-dependent kinase, are present in trypanosomes but diverge in function compared to other eukaryotes (5, 6).

The flagellum and its motility appear to play a key role in the control of cell division (7–9). This organelle initiates at the basal body, which is associated to the kinetoplast (10, 11), emerges from the flagellar pocket (FP), and it is attached along the cell body for most of its length by the flagellum attachment zone (FAZ). The flagellum contains a canonical axoneme and the paraflagellar rod (PFR) that are physically linked (12–14). The duplication and segregation of these structures are interdependent. During cytokinesis, the ingression of the cleavage furrow follows an axis in between the new and the old flagellum. The position and initiation of the furrow are closely related to the FAZ, as demonstrated by the study of flagellum mutants (15–21).

In eukaryotes such as yeasts or mammals the TOR pathway is a major player in the control of cell division mediated by the action of two protein complexes, TORC1 and TORC2 (22–25). These complexes contain the two different threonine/serine kinases TOR1 and TOR2 in the yeast *Saccharomyces cerevisiae* (26–28), and one TOR protein in mammals (29). TORC1 complex controls cell mass (25, 30–32) and TORC2 the spatial aspects of cell division through cytoskeleton formation (33, 34). The role of the TOR pathway was uncovered through its inhibition by rapamycin (35). This drug, as well as a compound termed FK506, binds a cytoplasmic protein termed FKBP12 (for FK506 binding protein of 12 kDa). Binding of these compounds to FKBP12 suppresses the enzymatic peptidylprolyl *cis/trans* isomerase (PPIase) activity of the protein (36, 37). The rapamycin/FKBP and FK506/FKBP then form ternary complexes with TOR and calcineurin, respectively (29, 30, 38, 39), leading to the inhibition of the downstream signal transduction pathways. FKBP12 binds and modulates the activity of several intracellular targets, such as the calcium channels ryanodine receptor (40) and inositol 1,4,5-triphosphate receptor (41, 42).

In trypanosomes, two TOR proteins have been identified (43–45). In BF, their respective functions seem to match those found in other eukaryotes. They are part of two different protein complexes with different cellular localizations. Gene knockdown of *TbTOR1* resulted in reduced cell growth and arrest in $G_1$ concomitant with reduced protein synthesis, whereas *TbTOR2* RNA interference (RNAi) induced abnormal morphology and cytokinesis defects generating cells with multiple flagella and nuclei. Finally, rapamycin inhibited cell

**Received** 7 March 2012 **Accepted** 19 October 2012
**Published ahead of print** 26 October 2012
Address correspondence to David Pérez-Morga, david.perez-morga@ulb.ac.be.
L.V. and D.P.-M. contributed equally to this article.
Supplemental material for this article may be found at http://dx.doi.org/10.1128/EC.00077-12.

doi:10.1128/EC.00077-12

growth through interference with TOR2 but not TOR1 formation. Recently, two novel TOR kinases, TbTOR3 and TbTOR4 (formerly TbTOR-like 1 and TbTOR-like 2) were identified in the genome of *T. brucei* (43). TbTOR3 is a cytoplasmic TOR kinase involved in polyphosphate metabolism, acidocalcisome maintenance (46), and virulence (47). TbTOR4 is involved in differentiation of slender into stumpy bloodstream forms (48).

We identified four members of the FKBP family and investigated their role in *T. brucei*. The knockdown of *FKBP12* was the only one to trigger detectable effects on trypanosomes in culture, with reduced motility in PF and impaired cytokinesis in BF. Remarkably, in BF the depletion of TbFKBP12 was associated with the presence of internal inside-out translucent cavities seemingly resulting from unsuccessful attempts of cell division. We propose that TbFKBP12 is a cytoskeleton-associated protein with BF-specific function in the FP region.

## MATERIALS AND METHODS

**Trypanosome culture and transfection.** The double-marker PF cell line 29-13 (49) was cultured at 27°C in SDM 79 medium containing 10% fetal calf serum. Cell density was kept at 1 to 10 million cells/ml by regular dilution, and growth curves are presented as cumulative data. Parasites were transfected as described previously (50). Briefly, cells were transfected with 5 μg of the linearized plasmid using a Bio-Rad Gene Pulser II. Cell lines were obtained by clonal dilution under selection with 5 μg of phleomycin/ml. For the induction of RNAi, cells were grown in the presence of 1 μg of fresh doxycycline (DOX)/ml.

The single-marker BF cell line 328-114 (49) was cultured at 37°C and 5% $CO_2$ in HMI-9 medium containing 10% fetal calf serum without tetracycline (Tet system approved fetal bovine serum; Clontech) (51). Cell density was maintained at 0.1 to 1 million cells/ml by regular dilution, and growth curves were presented as cumulative data. Parasites were transfected as described previously (52). Briefly, cells where transfected with 10 μg of the linearized plasmid using the AMAXA human T-cell nucleofector. Stably transfected clonal cell lines were recovered by selection with 1 μg of hygromycin/ml (RNAi) or with 1 μg of phleomycin/ml (complementation) in a 24-well plate. For induction of RNAi, cells were grown in the presence of 1 μg of fresh DOX/ml.

**Antibody production.** To obtain anti-FKBP12 antibodies, recombinant GST-TbFKBP12 was cloned in the pGEX4T1 vector (Amersham) and overexpressed in bacteria, purified in phosphate-buffered saline (PBS) on glutathione-Sepharose 4B (Amersham) beads and then injected into a mouse to produce polyclonal antisera.

**Plasmid construction. (i) RNAi.** The following primers were designed using Beacon Designer 7.0 (Premier Biosoft, CA) to PCR amplify a 331-nucleotide fragment of the 339 nucleotides, the *FKBP12* gene from wild-type *T. brucei* genomic DNA: TbFKBP12 F (5′-ATATGGATCCAAATGACTGC GTTATGATGG-3′) and TbFKBP12 R (5′-ATGCCTCGAGTCAAACAA CATCCAACAGCG-3′). PCR product was cloned in the p2T7*TiTA*177 vector (53). The sequence of the insert was verified by DNA sequencing (Genome Express), and the plasmid was then linearized by digestion with NotI before transfection.

**(ii) Complementation.** The chemical composition of a recoded open reading frame (ORF) coding for the TbFKBP12 protein was obtained from Entelechon. This sequence is synonymous to the *T. brucei TbFKBP12* gene but highly mutated: it has the same amino acid sequence but a different nucleotide sequence and is therefore not targeted by the RNAi machinery of the cell. The sequence (CTCGAGATGAGTAGGAAC GATTGTGTGATGATGGATAAAATAATCGAAGGTGACGGTAAGA CAATTCCTAGGCAAGGATCAATTGTTACGTTAGATTAC GTGGGGTACTTACCAGACGGAAGGAAATTTGATAGTACCATCG AGCGTGGAAAACCATTCGTGTTTAGGGTAGGTTGTGGCG AAGTGATTAAGGGTTGGGATGAAGGGATCGTTCAAATG AGCAAAGGAGAAAGGTCGAGATTGACTATGCCCCCGAG CTTAGCATTCGGTAGTACAGGATTTCCAGGGATTATCCC ACCGAATACGGTGATAGTTTTCGAAGTTACATTACTCG ACGTGGTCTAGAAGCTT) was cloned in a pTSA-rib vector (54) using the primers TbFKBP12-rev F (5′-ATATCTCGAGATGTCGCGAAATGA CTGCG-3′) and TbFKBP12-rev R (5′-ATATAAGCTTTCAAACAACAT CCAACAGCG-3′). This plasmid is targeted to a tubulin locus and allows a constitutive expression under the control of the ribosomal DNA promoter. The plasmid was linearized with BglII before transfection into the *TbFKBP12*$^{RNAi}$ cell line.

**qRT-PCR.** After RNAi induction RNAs from the BF and PF cells after RNAi induction were extracted with TRIzol (Invitrogen) and used as a template for reverse transcription with RT Superscript II (Invitrogen). The cDNAs were then amplified by quantitative reverse transcription-PCR (qRT-PCR) with specific primers for the *TbFKBP12* and histone H2B mRNAs using the SYBR green mix (ABgene).

**Electron microscopy.** For TEM, samples were fixed overnight at 4°C in 2.5% glutaraldehyde–0.1 M cacodylate buffer (pH 7.2) and postfixed in $OsO_4$ (2%) in the same buffer. After serial dehydration samples were embedded in Agar 100 (Agar Scientific, Ltd., United Kingdom) and left to polymerize at 60°C. Ultrathin sections (50 to 70 nm thick) were collected in Formvar-carbon-coated copper grids using a Leica EM UC6 ultramicrotome and stained with uranyl acetate and lead citrate. For immunogold detection by ultrathin cryosectioning, cells were fixed in 3% paraformaldehyde–0.5% glutaraldehyde–0.1 M cacodylate buffer (pH 7.2), embedded in 10% gelatin and 2.3 M sucrose, and frozen in liquid nitrogen. Sectioning of frozen samples was done on a Leica EM UC7 ultramicrotome. Sections on carbon-Formvar grids were probed with a mouse anti-TbFKBP12 antibody and an anti-mouse gold conjugate (5 nm) and then mounted in methylcellulose–1% uranyl acetate films. Observations were made on a Tecnai 10 electron microscope (FEI) and images were captured with a MegaView II camera and processed with AnalySIS and Adobe Photoshop software. For scanning electron microscopy (SEM), samples were fixed overnight at 4°C in 2.5% glutaraldehyde–0.1 M cacodylate buffer (pH 7.2) and postfixed in 2% $OsO_4$ in the same buffer. After serial dehydration, the samples were dried at a critical point and coated with platinum according to standard procedures. Observations were made in a Tecnai FEG ESEM Quanta 200 (FEI). For detergent extraction, the cells were treated with 1% Triton X-100 at 4°C in PBS for 10 min to strip the plasma membrane and to visualize the parasite cytoskeleton. Samples were washed twice in PBS, fixed in glutaraldehyde, and processed for SEM under standard conditions (55).

**Trypanosome cellular fractionation and Western analysis.** Trypanosomes lysates, detergent-soluble proteins, and cell cytoskeletons were prepared as described previously (56) and Western blotted as described previously (57). The primary antibody dilutions were as follows: monoclonal anti-trypanin, 1/2,500 (58); anti-enolase, 1/50,000 (59); and mouse polyclonal anti-TbFKBP12, 1/50.

**Immunofluorescence.** Cells were spread on poly-L-lysine-coated slides and either fixed and permeabilized in methanol at −20°C or fixed in 3.7% formaldehyde and then permeabilized in 0.01% Triton TX-100 before processing as described previously (60). Indirect immunofluorescence analyses were performed with mouse anti-TbFKBP12, anti-PFR2 antibody L8C4 (61), anti-FAZ antibody L3B2 (61), anti-acetylated α-tubulin (MAb 6-11b-1; Sigma), anti-TBBC antibody (basal body) (62), anti-enolase antibody (59), anti-trypanin antibody (58), and anti-BILBO1 antibody (63). The FP was labeled with Texas Red tomato-lectin (Vector Laboratories) (64). DNA was stained with DAPI (4′,6′-diamidino-2-phenylindole). Images were captured with a Zeiss Axioskop 2 coupled to a charge-coupled device camera (AxioCam HRM; Zeiss).

**Motility analyses.** For each stage, motility analysis was performed from two separate experiments. For each time point (0, 24, 48, and 72 h of induction), 16 to 20 movies were recorded (200 frames, 50 ms of exposure). Samples were observed in their respective media ($0.5 \times 10^6$ BF/ml of HMI-9 or $5 \times 10^6$ PF/ml of SDM 79) under the ×10 objective lens of an inverted DMI4000 Leica microscope coupled to a Retiga-SRV camera

(QImaging). Movies were converted with the mpeg Streamclip V.1.9b3 software (Squared 5) and analyzed using MedeaLAB CASA tracking V.5.5 software (Medea AV). For each movie, up to 199 cells were simultaneously tracked *in silico*. The studied parameters were as follows: curvilinear velocity (VCL; speed along the real path) and straight line velocity (VSL; speed calculated along the virtual linear path from the starting to the ending point). The data were transferred and compiled in Microsoft Excel, and statistical analyses were performed using KaleidaGraph v4.0 software (Synergy Software). The data were first filtered (number of frames, $>197$; $1\% < \text{linearity} < 99\%$; VSL $> 0.1$) to exclude incomplete and/or false. An analysis of variance test was then performed to study the effect of the RNAi induction over time on all of the measured parameters (Tukey ad hoc post test at 0.5 for intergroup comparisons; $P < 0.001$).

For a more precise analysis, ~20 movies of individual cells (200 frames, 100 ms of exposure) were recorded at different times after induction (0 and 48 h for BF; 0 and 72 h for PF). Samples were observed and processed as described above under a 100× NA 1.4 Plan Apo objective lens. A qualitative observation of each time-lapse movie was then performed to characterize flagellar beatings (wave orientation, beat amplitude, beat efficiency, and coordination of flagella).

## RESULTS

In *T. brucei*, computer-assisted BLAST analysis identified four matching sequences for the FKBP12 protein (see Fig. S1 in the supplemental material). Because of its size and highest level of identity, we focused in the present study on Tb927.7.3420, the putative homologue of FKBP12, which we termed TbFKBP12. At the amino acid level, TbFKBP12 shares 53 and 51% identities with the *S. cerevisiae* and the human homologue, respectively. The predicted 12.2-kDa protein (112 amino acids) contains a typical binding domain for the FK506 drug (FKBD), as well as a potential catalytic site for peptidylprolyl *cis-trans* isomerase (PPIase) activity (see Fig. S2 in the supplemental material). Despite the fact that the large majority of FKBPs display *in vitro* PPIase activity, we never succeeded to detect this activity in recombinant TbFKBP12 using classical synthetic prolyl-oligopeptide substrates (data not shown). The lack of detectable enzymatic activity could be related to the presence of several substitutions on key catalytic residues in the drug-binding pocket of TbFKBP12 that were proposed to mediate PPIase activity in other FKBPs (65) (asterisks in Fig. S2 in the supplemental material). Nevertheless, nuclear magnetic resonance (NMR) studies showed that the recombinant protein was correctly folded under the assay conditions and able to bind FK506 and rapamycin but apparently not the proline substrates, even to a concentration of 100 μM close to the $K_m$ for these peptides (290 μM; R. Aido-Machado, D. Salmon, and J. R. Pires, unpublished data). In addition, surface plasmon resonance analysis of the recombinant TbFKBP12-rapamycin interaction revealed an apparent $K_D$ (equilibrium dissociation constant) of 6.8 nM, slightly higher than that determined for the human FKBP12 (1.6 nM) (66; K. M. S. Kabral and D. Salmon, unpublished data). Although the overall structure of the FKBP is conserved, we speculated that the substitutions of some residues in TbFKBP12 including (Y87F and H92F) might be important in hydrogen bonding interaction within the active site of the enzyme (65), the lack of hydrogen bonds in both Phe substitutions could make the binding weaker with the peptide resulting in the loss of detectable PPIase activity (Aido-Machado et al., unpublished).

**Expression and localization of TbFKBP12.** Antibodies were produced against recombinant TbFKBP12 fused to a glutathione *S*-transferase (GST; N-terminal) tag. These antibodies specifically recognized a 12-kDa protein in *T. brucei* total cell extracts (lanes L, Fig. 1A). After cell fractionation, TbFKBP12 was found to be mainly associated with the cytoskeleton (lanes CK, Fig. 1A), while the control cytoplasmic enzyme enolase (59) and flagellar protein trypanin (58) were found in their respective expected fractions (Fig. 1A). Further experiments conducted to determine whether TbFKBP12 was associated with the cytoskeleton via subpellicular microtubules yielded inconsistent results (data not shown). Using indirect immunofluorescence assays (IFA), we found TbFKBP12 in a compartment juxtaposing the FP in BF (Fig. 1B). Frequently, the signal corresponding to TbFKBP12 in 1K1N cells had a bilobular aspect centered along the flagellum axis (Fig. 1B, arrow). Further colocalization experiments using tomato lectin as a marker for the FP lumen (64) and antibodies directed against BILBO1, an FP collar protein (63), confirmed the FP localization (Fig. 1C and D). Furthermore, these markers allowed us to define the relative position of TbFKBP12 at the posterior end, adjacent to BILBO1 and toward the interior of the cell. Using immunogold transmission electron microscopy (TEM) analysis on ultrathin cryosections, the gold label was often associated to an unidentified membrane network close to the posterior end of the cell and near the FP (see Fig. S3 in the supplemental material). In these cryosection pictures, the identification of the FP region was based on the presence of the axoneme, the PFR, the flagellum, FP membranes, and the FP collar. In contrast to membranes, cytoskeleton structures are poorly defined on cryosections. Despite numerous efforts, no consistent signal was detected in PF either by IFA or by immunogold analysis (data not shown).

***TbFKBP12* knockdown affects growth.** RNAi analysis was performed on PF and BF expressing the T7 phage RNA polymerase and the bacterial TET repressor (53). Knockdown of *TbFKBP12* was accomplished by the tetracycline-dependent expression of a *TbFKBP12*-specific double-stranded RNA (dsRNA) encoded on the p2T7*Ti*TA177 vector. Among the four *T. brucei* FKBP-related genes, only *TbFKBP12* knockdown led to a detectable phenotype. After RNAi-mediated reduction of both mRNA and protein TbFKBP12 levels (Fig. 2A to D), the growth of PF stopped after 3 days and that of BF after 1 day (Fig. 2). TbFKBP12 seemed to be less stable in PF than in BF, since after 3 days of RNAi induction the mRNA levels decreased to 81% in PF and to 78% BF, but the protein was still present in BF while not detected any longer in PF (Fig. 2A to D). To verify the specificity of the RNAi growth phenotype, we did a complementation analysis using a recoded sequence of *TbFKBP12* ORF called *FKBP12-rev*, which should be insensitive to RNAi but preserves the wild-type (WT) ORF. RT-PCR demonstrated efficient depletion of the endogenous *TbFKBP12*, whereas *TbFKBP12-rev* was strongly expressed and insensitive to RNAi as expected (see Fig. S4A in the supplemental material). This expression restored the normal growth (see Fig. S4B in the supplemental material), confirming the specificity of the phenotype.

**Cytokinesis is impaired in *TbFKBP12*$^{RNAi}$ cells.** To further define the growth-arrest phenotype upon knockdown of *TbFKBP12*, we counted the number of nuclei and kinetoplasts per cell after DAPI staining. The cell cycle progression in trypanosomes is easily followed from $G_1$ phase with 1 kinetoplast (K) and 1 nucleus (N), to $G_2$ phase with a 2K1N configuration that progresses into mitotic cells with 2K2N, which then splits into two daughter cells after cytokinesis (67).

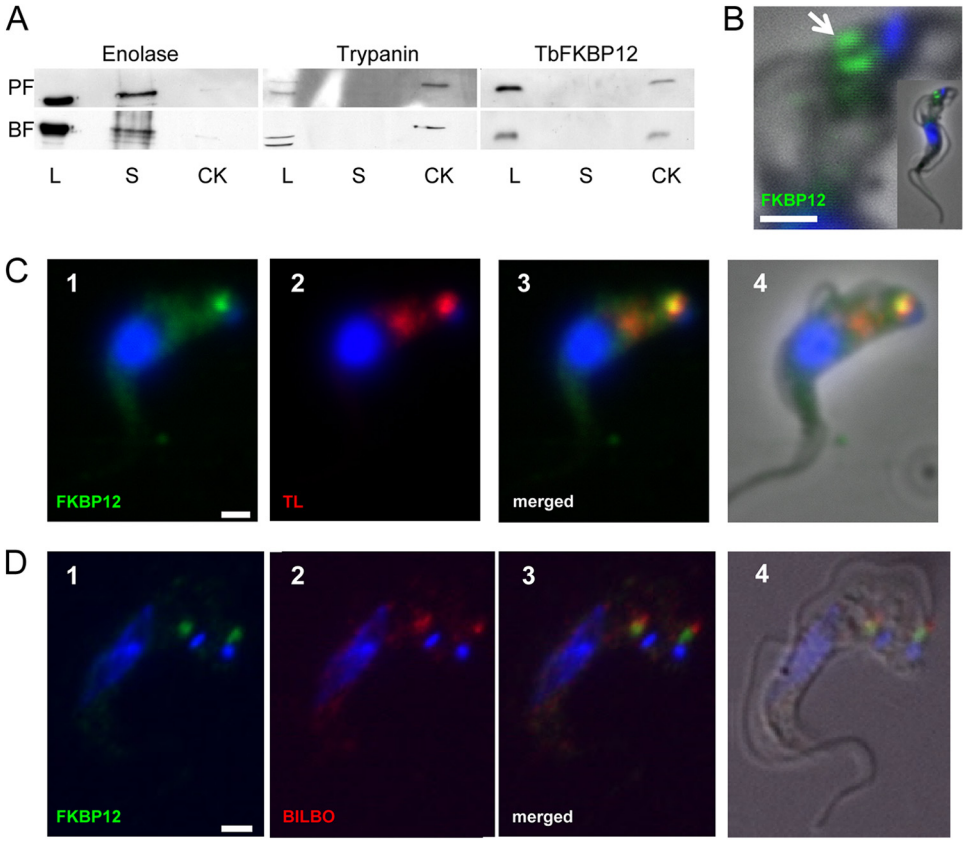


**FIG 1** TbFKBP12 subcellular localization. (A) Western blot probed with anti-TbFKBP12, anti-enolase, and anti-trypanin showing that TbFKBP12 is associated with the cytoskeleton of BF and PF. Enolase and trypanin are, respectively, control cytoplasmic and flagellar proteins. Whole-cell lysates (L) and soluble (S) and cytoskeletal (CK) fractions were prepared from wild-type BF or PF cells as described previously (11). (B) IFA of BF probed with mouse anti-TbFKBP12 (green). Superimposed images of DAPI DNA staining (blue) and phase-contrast images are also shown. (C) Tomato lectin (TL) and TbFKBP12 colocalization experiments. Panel 1, TbFKBP12 (green); panel 2, TL (red); panel 3, merged image of panels 1 and 2; panel 4, same as panel 3 plus DNA DAPI staining (blue) and phase-contrast images. (D) BILBO1 and TbFKBP12 colocalization experiments. Panel 1, TbFKBP12 (green); panel 2, BILBO1 (red) and DAPI staining (blue); panel 3, merged images of panels 1 and 2; panel 4, same as panel 3 plus a differential interference contrast image. Bar, 2 μm.

In PF, there were no major changes in the relative proportions of 1K1N, 2K1N, or 2K2N normal populations after 24 h of RNAi (Fig. 3A). However, all of these populations decreased progressively between 24 and 120 h, concomitantly with the emergence of cells with more than 2K2N whose abundance represented 20% of the population after 120 h of depletion.

In BF, the percentage of 1K1N and 2K1N cells remained relatively constant between 12 and 36 h after DOX addition, whereas the 2K2N population doubled during the first 6 h and then decreased to come back to its original value (Fig. 3B, light gray). During the same period we observed the emergence of a population of abnormal cells with more than 2K2N, which represented half of the population after 48 h of RNAi induction. The accumulation of more than 2 K and 2 N per cell indicated genome duplication but failure to complete cytokinesis. Thus, the growth arrest in BF was due to a failure in cytokinesis, in contrast to the PF situation. With a doubling time of 15 h for PF and 8 h for BF, six cell cycles correspond roughly to 90 h for PF and 48 h for BF. At these times, 21% of the PF population and 55% of the BF population were monster cells.

***TbFKBP12*$^{RNAi}$ cells present motility defects.** RNAi silencing of *TbFKBP12* specifically led to a motility defect in PF. This was first investigated by a standard sedimentation analysis (18). Upon depletion of TbFKBP12, PF sedimented at the bottom of the test flask within 4 h, which did not occur in BF (Fig. 4A and B). This motility defect was not responsible for the growth phenotype of PF, since shaking the culture did not reverse it, in contrast to other RNAi phenotypes causing reduced motility (8, 9; data not shown). Video microscopy revealed that the flagella of these cells were still beating, but this movement was not dragging cells in any particular direction (see Movie S1 to S3 in the supplemental material). In trypanosomes, the propulsive wave initiated from the anterior (tip) to the posterior (base) end of the flagellum drags the parasite forward and propagates with high frequency and low amplitude, whereas the reverse, base-to-tip wave, is used for changes in direction and propagates with low frequency and high amplitude (8, 9, 68). We analyzed several parameters for both PF and BF: (i) the curvilinear velocity (VCL, or speed along the real path), (ii) the straight-line velocity (VSL, or speed calculated along the virtual linear path from the starting to the ending point), (iii) the trajectory linearity (percentage of the total path), and (iv) the frequency of long and short stops. In PF all of these parameters progressively decreased along the time of TbFKBP12 depletion (Fig. 4C and data not shown). After 72 h, even though beats in

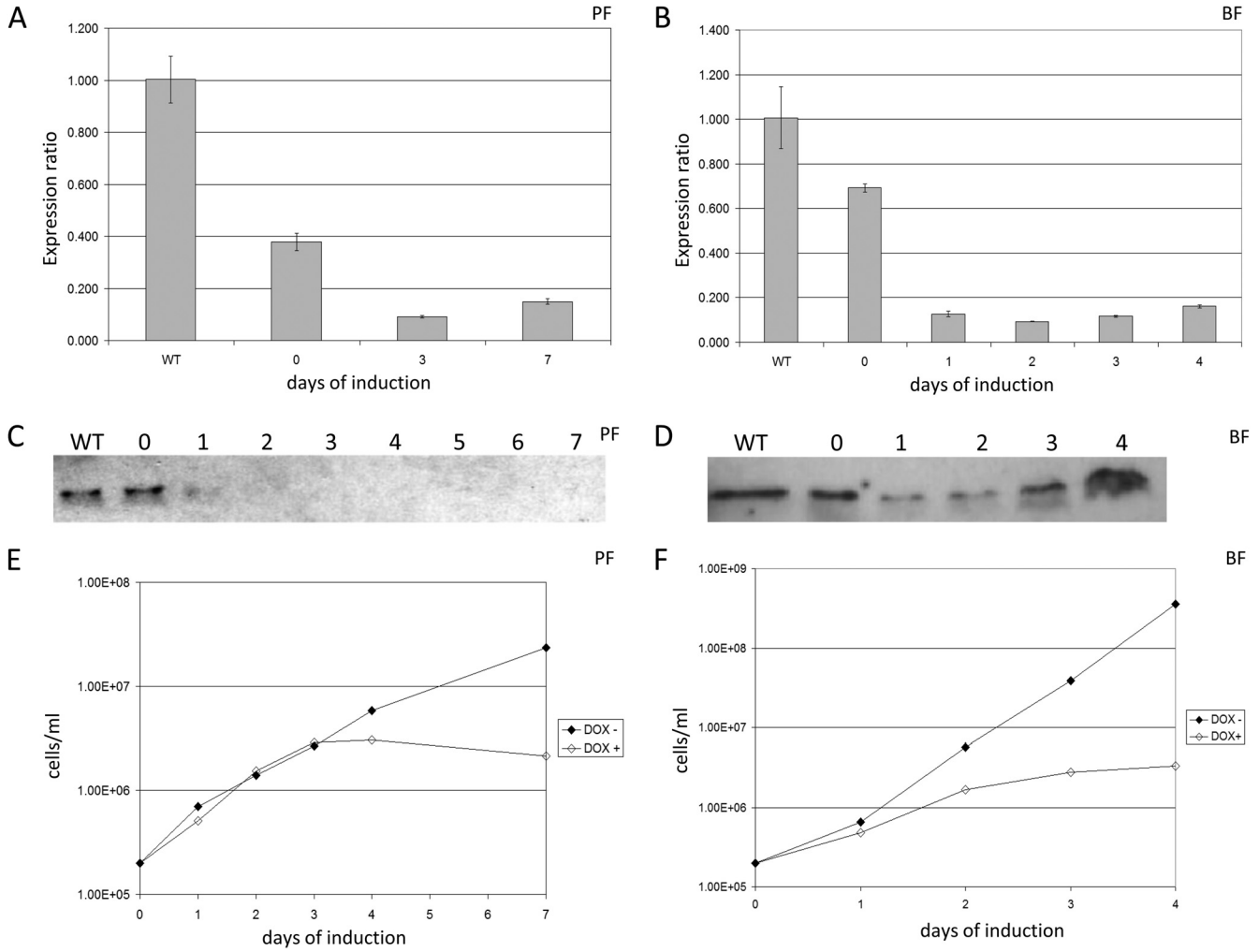


**FIG 2** TbFKBP12 is essential for parasite growth. (A and B) *TbFKBP12* mRNA expression in PF (A) and BF (B) *TbFKBP12*$^{RNAi}$ trypanosomes as evaluated by qRT-PCR. The expression of *TbFKBP12* mRNA was normalized to that of histone H2B (internal reference) and expressed as relative expression. (C and D) TbFKBP12 protein expression in PF(C) and BF(D) was evaluated by Western blotting with anti-TbFKBP12 antibody. Loading of equivalent amounts of protein was controlled by Ponceau red staining (data not shown). (E and F) Cumulative cell density growth curve of *TbFKBP12*$^{RNAi}$ PF (E) and BF (F), treated (DOX+, white lozenge) or not treated (DOX−, dark lozenge) with doxycycline. Cumulative cell densities are shown on a log scale as the product of the cell number and the total dilution at a given time.

both directions were observed, reverse waves (base to tip) were predominant, and propagation of the beats was often incomplete. In BF, no significant modifications were observed on these parameters up until 48 h after triggering RNAi (see Movies S4 to S7 in the supplemental material), when the velocity and distance covered on the whole decreased, although the linearity of the motility remained unchanged (Fig. 4D and data not shown). These effects were correlated with the increase in the number of multiflagellated cells with uncoordinated beating of their flagella and are in agreement with the sedimentation data. Overall, these results indicated that in PF the propulsive wave was affected, imposing a handicap on the parasite motility, whereas in BF reduced motility seemed mainly due to uncoordinated beating of multiple flagella in monster cells.

**Ultra-structural analysis of *FKBP12*$^{RNAi}$ PF cells.** Since cytokinesis is affected by defects in flagellum biogenesis (15–19), we analyzed the flagellum in TbFKBP12-depleted BF and PF cells. In both cell types, the formation of the paraflagellar rod (marked by an anti-PFR2 antibody), basal bodies (marked by the anti-TBBC antibody), and flagellar attachment zone (FAZ, marked by the anti-FAZ1 antibody) appeared normal upon depletion of TbFKBP12 (Fig. 5A). These images also showed the high number of flagella present in BF after 48 h of RNAi induction, paralleled by the accumulation of kinetoplasts and nuclei. The dual presence of flagellum-BB was still preserved, as well as that of the flagellum and the FAZ (Fig. 5A and data not shown).

In order to explore further a possible cause for the effect on motility, we used TEM and SEM for morphological analysis on *FKBP12*$^{RNAi}$ cells. TEM ultrastructural analysis confirmed the integrity of the flagella: the axoneme, the PFR, and the FAZ components were still present in *FKBP12*$^{RNAi}$ cells and showed the same inter-relationship as in WT cells (Fig. 5B). The 9+2 structure of the axoneme was preserved, together with the dynein arms and radial spokes.

We next analyzed the flagellum attachment to the cell body, since partial or complete detachment of the flagellum is one of the

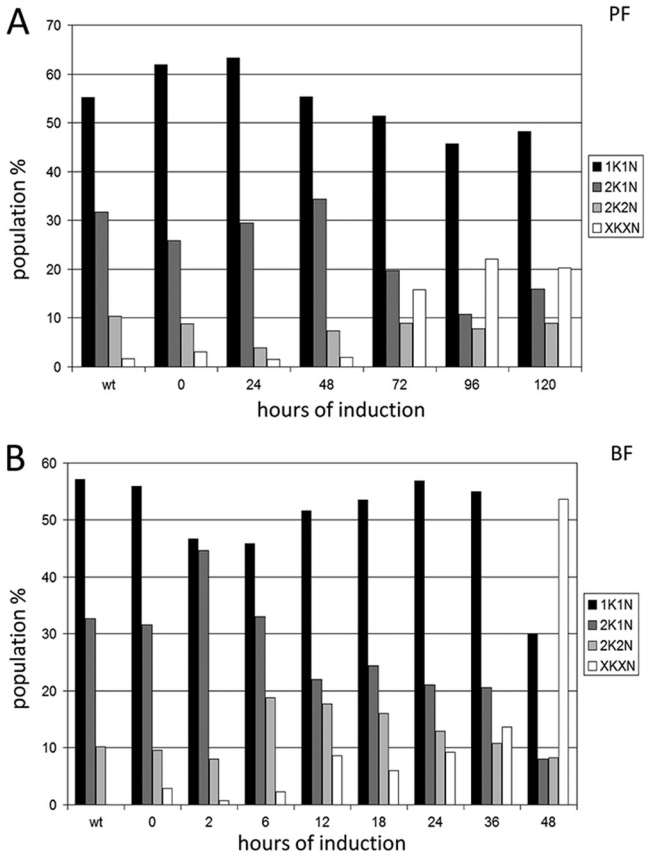


**FIG 3** DAPI staining analysis of the kinetoplast/nucleus content in PF (A) and BF (B) fixed cells. The percentages of 1K1N (dark), 2K1N (dark gray), 2K2N (gray) and of cells with multiple K and N (XKXN, white) are shown for wild-type parasites (wt) and for *TbFKBP12*$^{RNAi}$ and for cells after the indicated hours of doxycycline treatment. $N$ = at least 150 cells for each condition.

reported causes for lack of productive motility (69, 70). Using SEM and TEM, we did not observe alteration of flagellar attachment or anchorage to the cell body in *FKBP12*$^{RNAi}$ cells (data not shown). SEM cytoskeleton analysis of these parasites after membrane removal by detergent extraction (55) demonstrated several things. (i) The posterior region of the flagella appeared to be deeply encrusted in the cell body. (ii) Multiple cells were observed with unsegregated subpellicular microtubule (SPMT) networks, which were often associated at the middle of undivided cells (see Fig. S5C, panels 2 and 3, in the supplemental material). (iii) Some cells appeared to have abnormally separated from the posterior end or from both the anterior and the posterior ends. (iv) Finally, a low frequency of multiflagellated cells was observed with a complex and apparently unresolved SPMT network (see Fig. S5C, panel 3, in the supplemental material). Overall, these findings suggest that problems in flagellum attachment or positioning cannot account for the effects on motility of *FKBP12*$^{RNAi}$ PF cells and that cytoskeleton architecture is affected in these cells.

**Ultrastructural analysis of *FKBP12*$^{RNAi}$ BF reveals cell division defects.** Video microscopy on live BF arrested in cytokinesis showed that monster cells had a rosette-like morphology bearing several cell bodies of various sizes connected together at the posterior end (Fig. 6A). For simplicity, we refer to these monster cells as "aggregates," even though this does not mean individual cells that stuck together (see below). Each component of these monster cells still retained the streamline shape of normal cells and had one or several nonsynchronized motile flagella, and their body size was proportional to the number of flagella, nuclei, and kinetoplasts (Fig. 6A). By SEM we observed a rise in the number, size, and complexity of cell aggregates along the RNAi induction time (Fig. 6). The individual cells in these aggregates had a streamlined normal aspect, often with more than one flagellum (Fig. 6B, panels 2 to 4). The fact that the number and complexity of cell aggregates increased along the time of *TbFKBP12* RNAi induction indicated that these correspond to the rosette configurations observed by light microscopy. In TbFKBP12-depleted BF the flagellum exited at odd places along the cell body (Fig. 6B, panel 3, arrow). In contrast to PF, the flagellum was rarely detached from TbFKBP12-depleted BF. TEM analysis of cross-sections of *TbFKBP12*$^{RNAi}$ cells confirmed that the cell aggregates observed by light microscopy and SEM corresponded to a single massive undivided cell (Fig. 6C). In every instance one could discern the cell components in each of the multicellular bodies, since each one had the streamlined shape characteristic of trypanosomes and a peripheral flagellum transversal section (Fig. 6C, arrows). Altogether, these observations suggested that unresolved cell aggregates corresponded to late cytokinesis-arrested cells.

Intriguingly, TEM analysis of ultrathin sections revealed the presence of "cavities" at the interior of cytokinesis-arrested cells. These cavities had a translucent lumen limited by a wall of electron-dense material, of the same thickness and characteristics as the variant surface glycoprotein (VSG) coat, and an underlying array of microtubules equivalent to the SPMT (Fig. 7A, panel 1). These cavities of variable diameters (ranging from 27 to 986 nm, see Fig. S6A and B in the supplemental material) could be readily observed after 36 h (35%, $n$ = 82) and 48 h (40%, $n$ = 225) of RNAi induction in cross- and longitudinal sections. The cross-sections of the cavities were circular since their horizontal and vertical diameters were highly similar (see Fig. S6A in the supplemental material). In longitudinal sections, the length of cavities ranged from 87 to 3,834 nm (see Fig. S6C in the supplemental material). At 36 h of RNAi induction the cavities seemed to be longer and larger than at 48 h (see Fig. S6D in the supplemental material). The diameters of longitudinal sections were bigger than those measured on cross-sections (see Fig. S6A and B in the supplemental material). Statistical analysis of the size versus frequency distribution indicated that this was not Gaussian. Frequently, we observed several cavities of various diameters in the same cross-section, clearly following a common axis perpendicular to the central axis of the individual cavities (Fig. 7A, panel 2). Some cross-sections between two undivided cells showed strange cytokinesis configurations (Fig. 7B, panels 1 and 2, pointed lines). In several instances, the diameter of the cavities increased toward the cell interior; cavities of the smallest size were found near the cell surface (Fig. 7C, panels 1 to 4). In the example shown, we could clearly identify the VSG coat surrounded by 20-nm cross-sectioned microtubules (MT) (Fig. 7C, panels 1 to 3, red arrows), associated with membranes resembling those of the smooth endoplasmic reticulum (SER) surrounding the MT quartet of the FAZ (Fig. 7C, panel 4, white arrow). In some cases, there was a direct link between the ER from the FAZ and the MT of the cavities (Fig. 7C, panels 4 and 5, asterisks). This MT/ER association was

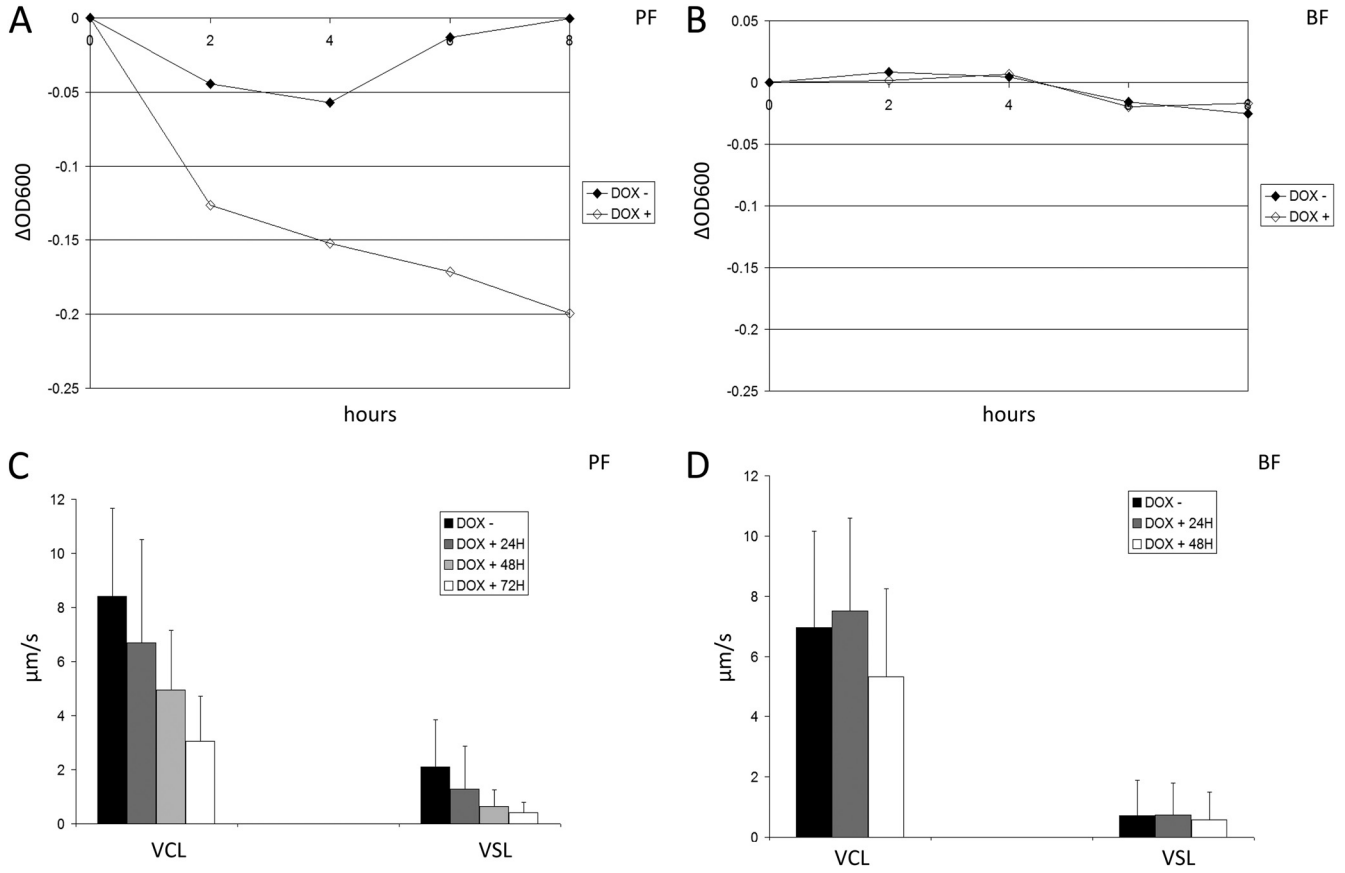


**FIG 4** Motility is modified in *TbFKBP12*$^{RNAi}$ parasites. Sedimentation assay on PF (A) and BF (B) *TbFKBP12*$^{RNAi}$ cells, treated (DOX+, white lozenge) and not (DOX−, dark lozenge) with doxycycline. The difference in the optical density at 600 nm before and after mixing the culture was recorded every 2 h after *TbFKBP12* RNAi induction for 60 h (PF) or 20 h (BF). The graph shown is representative of three different assays. Velocities of *TbFKBP12*$^{RNAi}$ PF (C) and BF (D) cells before (noninduced in black) and after induction (after 24 h in dark gray, 48 h in light gray, and 72 h in white) are indicated. The curvilinear (VCL) and linear (VSL) velocities are expressed in μm/s as their means and their standard deviations.

also observed in longitudinal sections (Fig. 7D), and it was particularly abundant at the posterior end of the cell (see below).

**Microtubules accumulation at the posterior end of *TbFKBP12*$^{RNAi}$ BF cells.** Since we had observed MT/ER associations particularly abundant at the posterior end of the RNAi BF cells (16.1% of cells with internal MT after 48 h of RNAi induction; $n = 118$) (Fig. 8A), we probed these cells for the presence of acetylated α-tubulin, which has been associated to MT biogenesis in BF (71). By IFA, we observed an increase (~10-fold, based on fluorescence intensity) of acetylated α-tubulin at the posterior end of *FKBP12*$^{RNAi}$ cells after 12 h of RNAi induction (70% of cells; $n = 108$) (Fig. 8B).

## DISCUSSION

Despite obvious phenotypic consequences of TbFKBP12 knockdown in both BF and PF, this protein did not show PPIase activity by standard assays. Since immunoprecipitation of the endogenous protein did not provide enough material, we could only use the recombinant version of TbFKBP12 to monitor its activity. This restriction cannot simply account for the lack of activity because NMR studies showed that the recombinant protein used for the assays is correctly folded and binds rapamycin and FK506 similarly to a control human protein. Therefore, PPIase activity might not be required for the physiological function of TbFKBP12, as was shown in both yeast and a pathogenic bacterium, *Burkholderia pseudomallei* (72, 73).

Proteins associated with FKBP12 have already been characterized in *T. brucei*, namely, TbTOR1, TbTOR2, TbTOR3, and TbTOR4 (43–48). TOR, FKBP, and rapamycin are in a tripartite complex, therefore interfering with TOR or FKBP could lead to similar phenotypes. Although TbTOR1 and TbTOR3 were found to be involved in cell cycle regulation and acidocalcisome maintenance, respectively, TbTOR2 was proposed to control cytokinesis and TbTOR4 was proposed to control slender to stumpy differentiation. However, the *TbTOR2* knockdown phenotype differed from that exhibited by *TbFKBP12*$^{RNAi}$ cells. We did not observe the FP swelling phenotype, while the intracellular cavities of the *TbFKBP12*$^{RNAi}$ cells were not observed in previous studies (45).

Fractionation experiments on detergent-extracted cells demonstrated the presence of TbFKB12 in the cytoskeleton fraction. However, we could not identify the cytoskeleton component to which TbFKBP12 is associated. In BF, TbFKBP12 was localized to a region adjacent to the FP collar, where it might be associated with an unidentified membrane compartment. Several cytoskeleton components are located near the FP zone, namely, the basal bodies and associated filaments, the MT quartet associated to the FAZ and the FP collar (74). The fenestrated endoplasmic reticu-

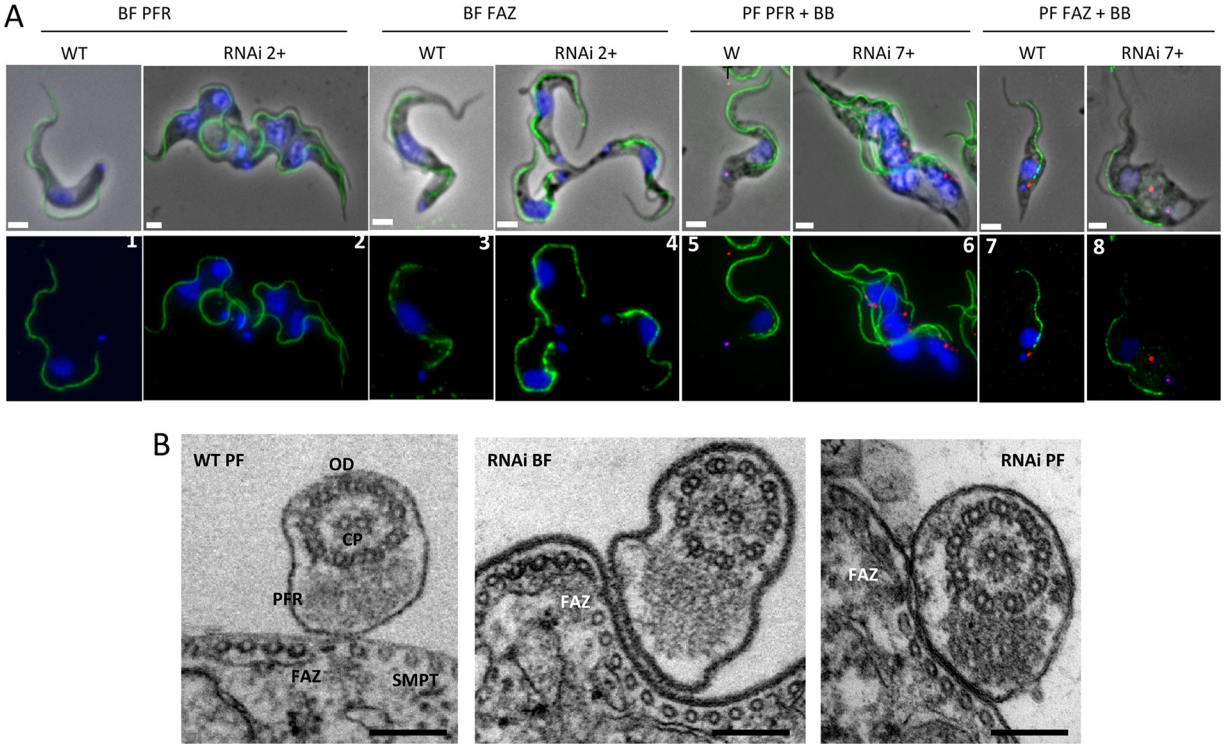


**FIG 5** Flagellum structure is not visibly affected in *TbFKBP12*$^{RNAi}$ cells. (A) IFA of BF and PF WT or *TbFKBP12*$^{RNAi}$ cells (RNAi+) 2 or 7 days after RNAi induction. Nuclei and kinetoplasts are stained in blue with DAPI. Cytoskeleton components are labeled in green with antibodies: L8C4 for the PFR and L3B2 for the flagellar attachment zone (FAZ). The basal bodies are labeled with anti-TBBC in red. Merged images plus or minus the phase contrast are presented. Bars, 2 μm. (B) Representative TEM images of flagella from WT and *TbFKBP12*$^{RNAi}$ after 2 days of RNAi induction in BF (RNAi BF) or 4 days in PF (RNAi PF). The PFR, FAZ and associated filaments, SPMT, and central pair (CP) and outer doublets (OD) of the axoneme are present in *TbFKBP12*$^{RNAi}$ cells. Bars, 200 nm.

lum (FER) identified by TEM tomography (74, 75) is a good candidate for the TbFKBP12-containing compartment, but this hypothesis is difficult to assess in the absence of specific marker to label the FER. We propose that the bulk of TbFKBP12 is associated with the cytoskeleton in both PF and BF, whereas only in BF would a fraction be located in the FP region. The higher local concentration of TbFKBP12 at the FP region of BF would account for its detection in this location only, whereas its absence from the FP of PF would explain the differential RNAi phenotype between PF and BF.

While *FKBP12* is nonessential in yeast (76), TbFKBP12 was required for both PF and BF growth. In neither PF nor BF was biogenesis of the flagellum or of any other cell organelle analyzed affected. Regarding the flagellum, all of its main components, as analyzed by IFA and EM, appeared to be normal in *FKBP12*$^{RNAi}$ cells. In PF the loss of TbFKBP12 affected motility, with a quick drop in curvilinear velocity due to a loss of coordination in the production of propulsive and reverse waves. This is translated in the rapid cessation of productive movement that causes cells to sediment in the culture flask within 60 h of RNAi induction. We ignored the primary cause for this effect on motility, but it does not seem to be related to an obvious loss of flagellar components or to flagellar detachment or flagellum anchoring. Calcium movement is a process that could be targeted very fast. Within this context, flagellar tip-to-base and base-to-tip waves have been shown to depend on different calcium concentrations on isolated flagella from the trypanosomatid *Crithidia oncopelti* (77). Furthermore, $Ca^{2+}$ movement in sperm flagella and cilia is controlled through the modulation of IP3R and RyR in the ER, both ligands of FKBP12 (78, 79). Another possibility is that cytoskeleton organization (flagellum and/or SPMT) in *TbFKBP12*$^{RNAi}$ PF might indeed be affected. Differences in cell body shape are correlated with a diverse range of cell behaviors contributing to the directional motion of the cell. For instance, straighter cells swim more directionally, whereas cells that exhibit little net displacement appear to be more bent (80). Because the flagellum is attached laterally along the length of the cell body, a helical wave of the flagellum necessarily applies a torsional stress to the cell body. Depending on the degree of viscoelasticity of the cell body, the cell body may well be able to store a significant amount of torsional elastic energy in reversible deformation of the microtubule cytoskeleton. This elastic energy could then be released when the flagellum started to rotate in the opposite direction (68). A disorganization of the cytoskeletal microtubule network could prevent proper storage or release of this elastic energy and consequently impair the parasite motion.

Contrary to the effects seen in PF, in BF the motility defects were only observed after long periods of RNAi induction, and they were associated with uncoordinated beating of the multiple flagella of undivided cells. Consequently, the main phenotype of BF was the inhibition of cytokinesis with no effect on mitosis, leading to the accumulation of monster cells bearing multiple flagella, kinetoplasts, and nuclei similar to previously described phenotypes linked to the invalidation of some flagellar components (8, 9,

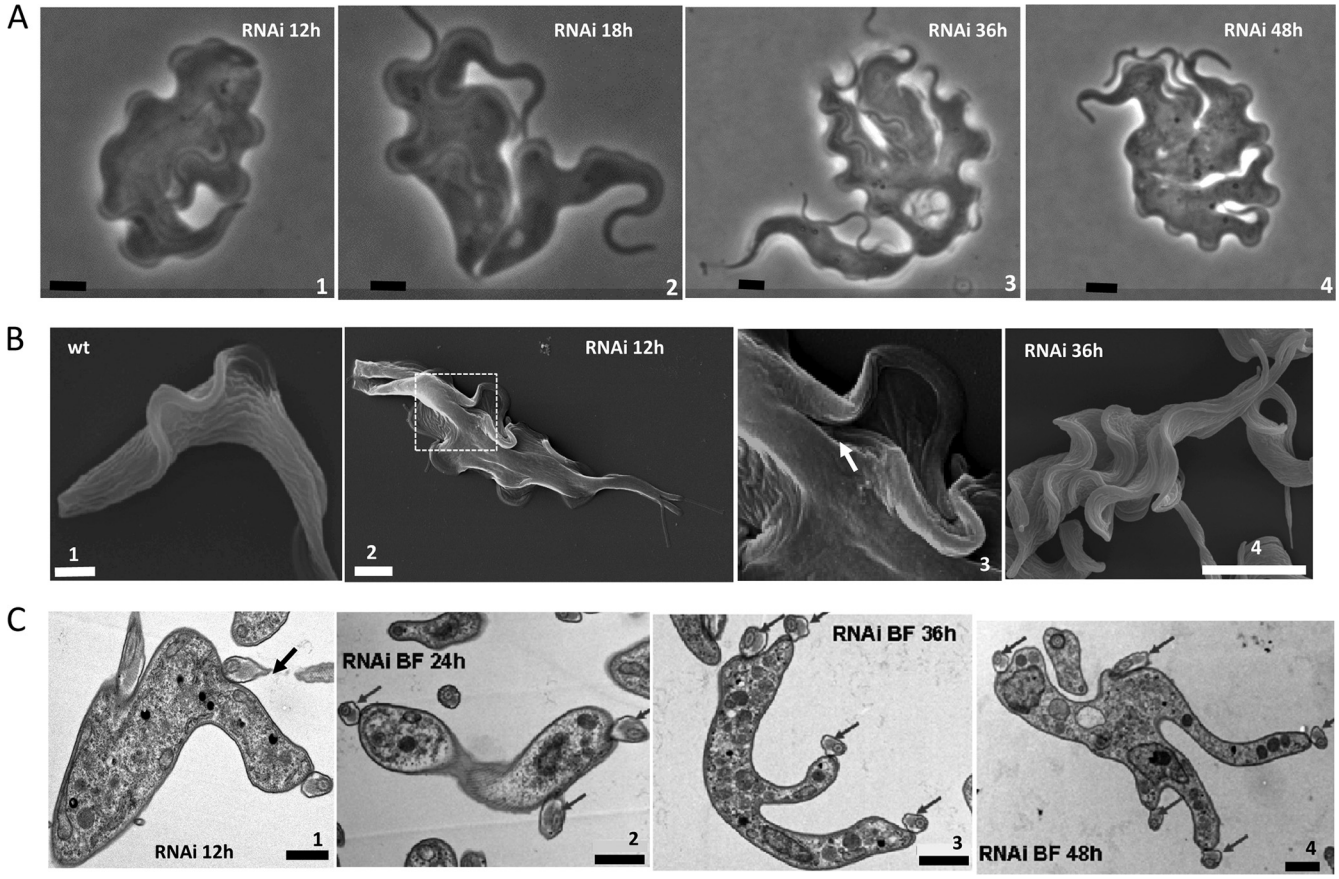


**FIG 6** Representative images of WT or *TbFKBP12*$^{RNAi}$ BF cells (RNAi) as observed by phase-contrast microscopy on living cells (A) and SEM (B). *TbFKBP12*$^{RNAi}$ cells are multiflagellated and show a rosette-like morphology. (C) TEM images show cross-sections of massive cells that may correspond to the rosette-like morphology observed in panels A and B. The cell body components of the rosettes are always associated to a peripheral flagellum (dark arrows). Subpanel 3 in panel B is an enlargement of the boxed area in subpanel 2; a white arrow points to a flagellum exiting abnormally. Bars: 4 μm (A), 2 μm (B, except subpanel 4, where it represents 5 μm), and 2 μm (C).

58, 81). Given the frequency and the diversity of cell processes were this phenotype has been observed, it might be directly or indirectly related to cytokinesis (6, 71). To our knowledge, the presence of cavities limited by a wall composed of MT, a plasma membrane, and a VSG coat has not been reported in any of the cytokinesis-arrested phenotypes. Neither have we ever seen similar features in our vast collection of RNAi mutants and trypanosomes under deleterious physiological conditions, even after long injury periods (4 to 6 days). We therefore concluded that the presence of cavities is specific to the ablation of TbFKBP12 and that the effect on cytokinesis is potentially due to the disruption of cytoskeleton dynamics. The analysis of hundreds of images led us to the conclusion that the cavities are ellipsoids in shape and run along the longitudinal axis of the cell. When multiple, the cavities were not randomly distributed in the cytoplasm but rather aligned along a foresighted division axis. Cross-sections of the smallest cavities showed that their microtubules were associated to a membrane similar to the smooth endoplasmic reticulum (SER), which could provide the membrane lining the cavities. Based on all of these data, we favor a working model for the generation of these cavities (Fig. 9). VSG coats, SPMTs, and SER membranes are nucleated and formed on the cytoplasmic side of the cell surface and, from then on, they move inward at the same time as more MTs are joining to increase the cavity diameter and length. This process then progresses on the longitudinal axis of the cell to form streamlined cavities. Interestingly, SPMTs seemed to seed the formation of cavities and to leave behind a region deprived of them at the cell surface. The existence of extensive amounts of MTs bound to SER inside these cells led us to conclude that there is a very active process to generate them and that these SER-associated MTs provide the necessary MTs and membranes to generate the cavities. Accordingly, the cavities may inherit the SPMT spatial patterning from their harboring cells through the lateral seeding of newly formed microtubules on preexisting SPMTs. A similar process has been previously suggested (82). We propose that these cavities result from unsuccessful attempts of cell abscission; when multiple, they reflect an uncontrolled and redundant command for a cytokinesis event involving the construction of a surface coat (Fig. 9C). Since we consistently observed these cavities between two flagella, it is possible that two neighboring, mislocalized flagella may signal the formation of a cleavage furrow between them and promote the formation of internal MT cytoskeletons (Fig. 9B and D). It has been proposed that the correct positioning of the new and old flagella is necessary to define cellular pattern (83, 84). This could occur through the flagellar connector (FC), a small structure that maintains the distal tip of the new flagellum in perma-

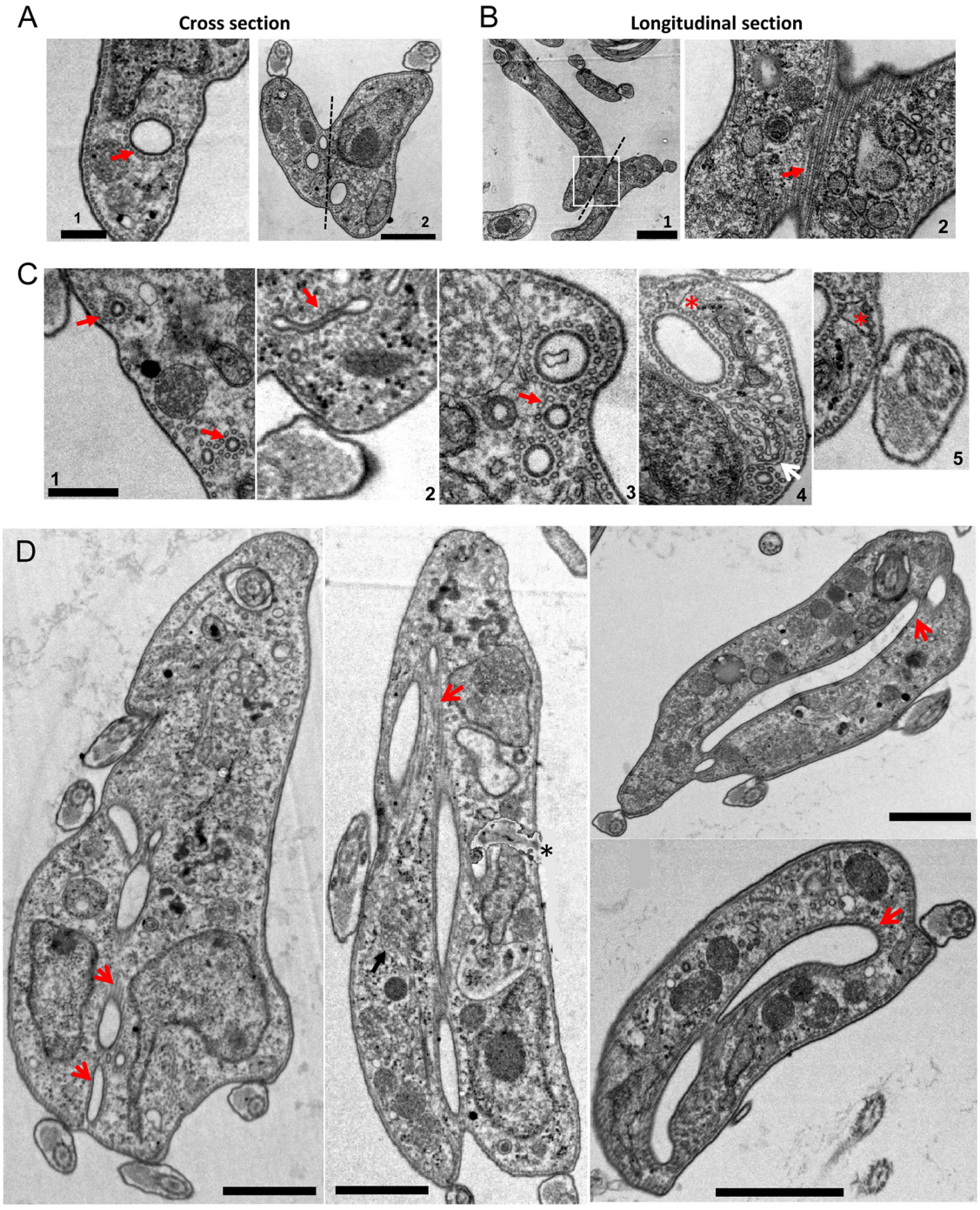


**FIG 7** TEM analysis of cavities in *TbFKBP12*$^{RNAi}$ BF cells. Cavities can be observed in cross-sections (A and C) and longitudinal sections (B and D). When multiple, they follow a foresight division axis (dashed line) between cell bodies. Cavities are outlined by a surface similar to the plasma membrane, composed of VSG and MTs similar to SPMT. (C) The smallest cavities are found near the plasma membrane and surrounded by MTs (red arrows) associated with smooth endoplasmic reticulum (white arrow, panel 4) or derived from the SPMTs. Red asterisks show the ER from the FAZ linked to the MT in some cavities. Subpanel 2 in panel B is an enlargement of the boxed area in subpanel 1. Bars: 200 nm (A and C), 1 μm (B and D). RNA induction times: 36 h (A to D) and 48 h (D). *, Dirt speck digitally filtered.

nent contact with the side of the old flagellum. Within this context it is important to mention that in several instances, we observed a direct association between the FAZ ER and some of the MTs lining the cavities, which might be relevant giving the importance of the FAZ in defining cell polarity (85, 86).

How do the observed effects relate to the location of TbFKBP12 in BF? One possibility is that this protein regulates the formation of the SPMT cytoskeletons at the posterior end of BF cells. As mentioned above, TbFKBP12 might be located in the fenestrated endoplasmic reticulum, which, incidentally, re-

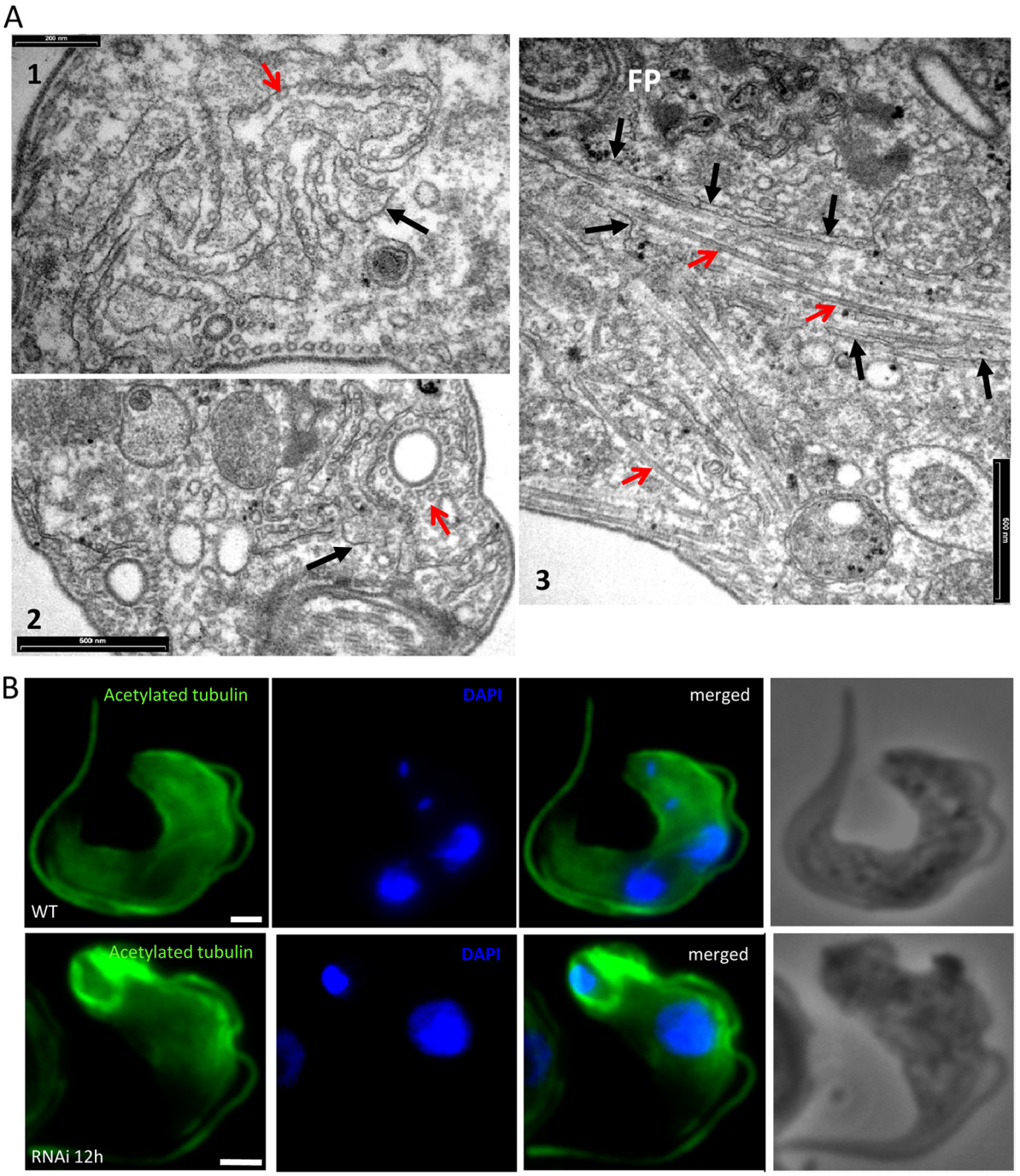


**FIG 8** Microtubules accumulation at the posterior end of *TbFKBP12*$^{RNAi}$ BF cells. (A) TEM images of *TbFKBP12*$^{RNAi}$ BF cells 48 h after RNAi induction. Red arrows: microtubules, black arrows: ER-like membranes. Bars: panel 1: 200 nm, panels 2 and 3: 500 nm. (B) Acetylated α-tubulin (green) localization in WT and *TbFKBP12*$^{RNAi}$ BF cells 12 h after RNAi induction. DAPI staining of kinetoplast DNA and nuclei (blue) is shown together with merged images. Bar, 2 μm.

sembles the membranes associated with the MTs fed to the cavities. The hypothesis that TbFKBP12 might regulate *de novo* SPMT cytoskeleton formation at the posterior end is indirectly supported by two observations. First, there is an accumulation of acetylated α-tubulin and microtubules at the posterior ends of RNAi BF cells. To our knowledge, the accumulation of free MTs in trypanosomes has not been reported in any situation. Second, a similar deposition of α-tubulin at the posterior end has been observed in PF for tyrosinated α-tubulin (60, 85) but not for its acetylated form (87). Importantly, the assembly of newly synthesized SPMTs occurs at the posterior ends of PF cells (60, 85, 87) and, more recently, the acetylation of α-tubulin has been associated with MT biogenesis in BF cells (71). Therefore, the acetylated α-tubulin accumulation at the poste-

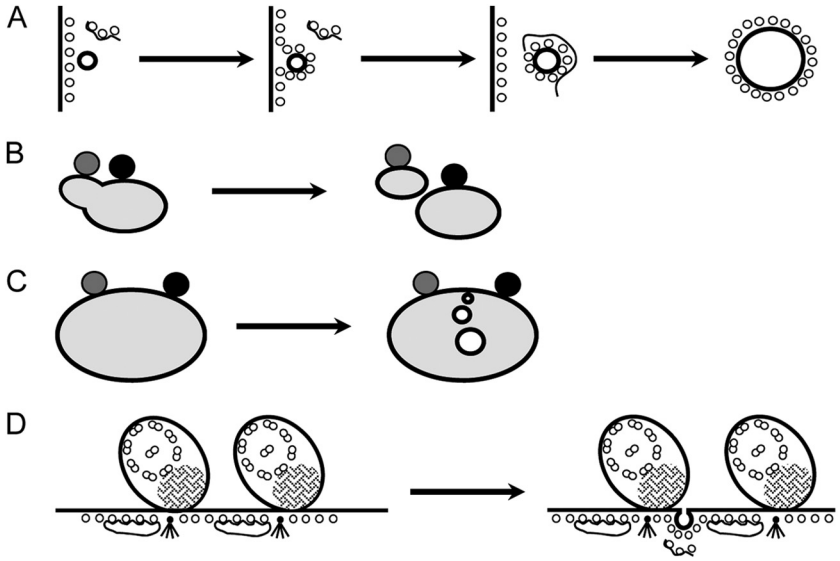


**FIG 9** Working model for cavity formation in *TbFKBP12*$^{RNAi}$ BF cells. (A) First events in the formation of the cavities. Dark thick line circles represent the VSG coat, thin line circles represent microtubules, and the wavy line represents the smooth endoplasmic reticulum. (B and C) Cross-sections at the posterior end of a dividing cell in a WT situation and in *TbFKBP12*$^{RNAi}$ cells, respectively. The filled dark circles represent the old flagellum, while the gray one represents the new one. The big light gray oval represents the cell body. Note the distance that separates the tips of both flagella before and after the initiation of cytokinesis (events separated by an arrow). Internal empty circles represent the cavities. (D) Formation of cavities, as depicted in panel A, at the interflagellar region. All views are from the posterior end of the cell.

rior ends of *TbFKBP12*$^{RNAi}$ BF cells represents an early event related to MT neogenesis prior to cavity formation.

Further work is obviously needed to establish the nature of the TbFKBP12-containing region and the function of the protein and to define the architecture of the observed cavities in three dimensions by TEM tomography, which may provide clues as to how cytoskeleton formation and cytokinesis occurs in trypanosomes.

## ACKNOWLEDGMENTS

This study was supported by the Belgian Fund for Scientific Research and the Interuniversity Attraction Poles Program–Belgian Science Policy. The CMMI is supported by the European Regional Development Fund and the Walloon Region. Work at the Pasteur Institute was funded by the Pasteur Institute, the CNRS, and a grant from the ANR (08-MIE-027).

We thank Keith Gull (Oxford University, United Kingdom) for antibodies and Frédéric Fontaine, Noémie Lepage, Laurence Lecordier, and Daniel Monteyne for assistance. A.B. was financed by FRIA, and B.R. is funded by a Roux postdoctoral fellowship.

## REFERENCES

1. **Vickerman K.** 1985. Developmental cycles and biology of pathogenic trypanosomes. Br. Med. Bull. **41**:105–114.
2. **Hammarton TC, Clark J, Douglas F, Boshart M, Mottram JC.** 2003. Stage-specific differences in cell cycle control in *Trypanosoma brucei* revealed by RNA interference of a mitotic cyclin. J. Biol. Chem. **278**:22877–22886.
3. **Kumar P, Wang CC.** 2006. Dissociation of cytokinesis initiation from mitotic control in a eukaryote. Eukaryot. Cell **5**:92–102.
4. **Ploubidou A, Robinson DR, Docherty RC, Ogbadoyi EO, Gull K.** 1999. Evidence for novel cell cycle checkpoints in trypanosomes: kinetoplast segregation and cytokinesis in the absence of mitosis. J. Cell Sci. **112**:4641–4650.
5. **Hammarton TC.** 2007. Cell cycle regulation in *Trypanosoma brucei*. Mol. Biochem. Parasitol. **153**:1–8.
6. **Hammarton TC, Monnerat S, Mottram JC.** 2007. Cytokinesis in trypanosomatids. Curr. Opin. Microbiol. **10**:520–527.
7. **Baron DM, Kabututu ZP, Hill KL.** 2007. Stuck in reverse: loss of LC1 in *Trypanosoma brucei* disrupts outer dynein arms and leads to reverse flagellar beat and backward movement. J. Cell Sci. **120**:1513–1520.
8. **Branche C, Kohl L, Toutirais G, Buisson J, Cosson J, Bastin P.** 2006. Conserved and specific functions of axoneme components in trypanosome motility. J. Cell Sci. **119**:3443–3455.
9. **Ralston KS, Lerner AG, Diener DR, Hill KL.** 2006. Flagellar motility contributes to cytokinesis in *Trypanosoma brucei* and is modulated by an evolutionarily conserved dynein regulatory system. Eukaryot. Cell **5**:696–711.
10. **Ogbadoyi EO, Robinson DR, Gull K.** 2003. A high-order transmembrane structural linkage is responsible for mitochondrial genome positioning and segregation by flagellar basal bodies in trypanosomes. Mol. Biol. Cell **14**:1769–1779.
11. **Robinson DR, Gull K.** 1991. Basal body movements as a mechanism for mitochondrial genome segregation in the trypanosome cell cycle. Nature **352**:731–733.
12. **Bastin P, Pullen TJ, Moreira-Leite FF, Gull K.** 2000. Inside and outside of the trypanosome flagellum: a multifunctional organelle. Microbes Infect. **2**:1865–1874.
13. **Ralston K, Kabututu Z, Melehani J, Oberholzer M, Hill K.** 2009. The *Trypanosoma brucei* flagellum: moving parasites in new directions. Annu. Rev. Microbiol. **63**:335–362.
14. **Vaughan S, Gull K.** 2003. The trypanosome flagellum. J. Cell Sci. **116**:757–759.
15. **Absalon S, Blisnick T, Kohl L, Toutirais G, Dore G, Julkowska D, Tavenet A, Bastin P.** 2008. Intraflagellar transport and functional analysis of genes required for flagellum formation in trypanosomes. Mol. Biol. Cell **19**:929–944.
16. **Bastin P, Gull K.** 1999. Assembly and function of complex flagellar structures illustrated by the paraflagellar rod of trypanosomes. Protist **150**:113–123.
17. **Bastin P, MacRae TH, Francis SB, Matthews KR, Gull K.** 1999. Flagellar morphogenesis: protein targeting and assembly in the paraflagellar rod of trypanosomes. Mol. Cell. Biol. **19**:8191–8200.
18. **Bastin P, Pullen TJ, Sherwin T, Gull K.** 1999. Protein transport and flagellum assembly dynamics revealed by analysis of the paralyzed trypanosome mutant snl-1. J. Cell Sci. **112**:3769–3777.

19. **Davidge JA, Chambers E, Dickinson HA, Towers K, Ginger ML, McKean PG, Gull K.** 2006. Trypanosome IFT mutants provide insight into the motor location for mobility of the flagella connector and flagellar membrane formation. J. Cell Sci. **119**:3935–3943.
20. **Franklin JB, Ullu E.** 2010. Biochemical analysis of PIFTC3, the *Trypanosoma brucei* orthologue of nematode DYF-13, reveals interactions with established and putative intraflagellar transport components. Mol. Microbiol. **78**:173–186.
21. **Kohl L, Robinson D, Bastin P.** 2003. Novel roles for the flagellum in cell morphogenesis and cytokinesis of trypanosomes. EMBO J. **22**:5336–5346.
22. **Crespo J, Hall M.** 2002. Elucidating TOR signaling and rapamycin action: lessons from *Saccharomyces cerevisiae*. Microbiol. Mol. Biol. Rev. **66**:579–591.
23. **Martin DE, Hall MN.** 2005. The expanding TOR signaling network. Curr. Opin. Cell Biol. **17**:158–166.
24. **Jaeschke A, Dennis PB, Thomas G.** 2004. mTOR: a mediator of intracellular homeostasis. Curr. Top. Microbiol. Immunol. **279**:283–298.
25. **Wullschleger S, Loewith R, Hall MN.** 2006. TOR signaling in growth and metabolism. Cell **124**:471–484.
26. **Helliwell S, Wagner P, Kunz J, Deuter-Reinhard M, Henriquez R, Hall M.** 1994. TOR1 and TOR2 are structurally and functionally similar but not identical phosphatidylinositol kinase homologues in yeast. Mol. Biol. Cell **5**:105–118.
27. **Loewith R, Jacinto E, Wullschleger S, Lorberg A, Crespo J, Bonenfant D, Oppliger W, Jenoe P, Hall M.** 2002. Two TOR complexes, only one of which is rapamycin sensitive, have distinct roles in cell growth control. Mol. Cell **10**:457–468.
28. **Wedaman K, Reinke A, Anderson S, Jr. Yates McCaffery J, Powers T.** 2003. Tor kinases are in distinct membrane-associated protein complexes in *Saccharomyces cerevisiae*. Mol. Biol. Cell **14**:1204–1220.
29. **Sabatini D, Erdjument-Bromage H, Lui M, Tempst P, Snyder S.** 1994. RAFT1: a mammalian protein that binds to FKBP12 in a rapamycin-dependent fashion and is homologous to yeast TORs. Cell **78**:35–43.
30. **Cardenas ME, Hemenway C, Muir RS, Ye R, Fiorentino D, Heitman J.** 1994. Immunophilins interact with calcineurin in the absence of exogenous immunosuppressive ligands. EMBO J. **13**:5944–5957.
31. **Noda T, Ohsumi Y.** 1998. Tor, a phosphatidylinositol kinase homologue, controls autophagy in yeast. J. Biol. Chem. **273**:3963–3966.
32. **Powers T, Walter P.** 1999. Regulation of ribosome biogenesis by the rapamycin-sensitive TOR-signaling pathway in *Saccharomyces cerevisiae*. Mol. Biol. Cell **10**:987–1000.
33. **Jacinto E, Loewith R, Schmidt A, Lin S, Rüegg MA, Hall A, Hall MN.** 2004. Mammalian TOR complex 2 controls the actin cytoskeleton and is rapamycin insensitive. Nat. Cell Biol. **6**:1122–1128.
34. **Schmidt A, Kunz J, Hall MN.** 1996. TOR2 is required for organization of the actin cytoskeleton in yeast. Proc. Natl. Acad. Sci. U. S. A. **93**:13780–13785.
35. **Heitman J, Movva NR, Hall MN.** 1991. Targets for cell cycle arrest by the immunosuppressant rapamycin in yeast. Science **253**:905–909.
36. **Harding MW, Galat A, Uehling DE, Schreiber SL.** 1989. A receptor for the immunosuppressant FK506 is a *cis-trans* peptidyl-prolyl isomerase. Nature **341**:758–760.
37. **Siekierka JJ, Hung SH, Poe M, Lin CS, Sigal NH.** 1989. A cytosolic binding protein for the immunosuppressant FK506 has peptidyl-prolyl isomerase activity but is distinct from cyclophilin. Nature **341**:755–757.
38. **Chiu M, Katz H, Berlin V.** 1994. RAPT1, a mammalian homolog of yeast Tor, interacts with the FKBP12/rapamycin complex. Proc. Natl. Acad. Sci. U. S. A. **91**:12574–12578.
39. **Liu J, Farmer JD, Jr, Lane WS, Friedman J, Weissman I, Schreiber SL.** 1991. Calcineurin is a common target of cyclophilin-cyclosporine and FKBP-FK506 complexes. Cell **66**:807–815.
40. **Chelu MG, Danila CI, Gilman CP, Hamilton SL.** 2004. Regulation of ryanodine receptors by FK506 binding proteins. Trends Cardiovasc. Med. **14**:227–234.
41. **Cameron AM, Nucifora FC, Jr, Fung ET, Livingston DJ, Aldape RA, Ross CA, Snyder SH.** 1997. FKBP12 binds the inositol 1,4,5-trisphosphate receptor at leucine-proline (1400–1401) and anchors calcineurin to this FK506-like domain. J. Biol. Chem. **272**:27582–27588.
42. **Cameron AM, Steiner JP, Roskams AJ, Ali SM, Ronnett GV, Snyder SH.** 1995. Calcineurin associated with the inositol 1,4,5-trisphosphate receptor-FKBP12 complex modulates $Ca^{2+}$ flux. Cell **83**:463–472.
43. **Barquilla A, Crespo JL, Navarro M.** 2008. Rapamycin inhibits trypanosome cell growth by preventing TOR complex 2 formation. Proc. Natl. Acad. Sci. U. S. A. **105**:14579–14584.
44. **Barquilla A, Navarro M.** 2009. Trypanosome TOR as a major regulator of cell growth and autophagy. Autophagy **5**:256–258.
45. **Barquilla A, Navarro M.** 2009. Trypanosome TOR complex 2 functions in cytokinesis. Cell Cycle **8**:697–699.
46. **de Jesus TC, Tonelli RR, Nardelli SC, da Silva Augusto L, Motta MC, Girard-Dias W, Miranda K, Ulrich P, Jimenez V, Barquilla A, Navarro M, Docampo R, Schenkman S.** 2010. Target of rapamycin (TOR)-like 1 kinase is involved in the control of polyphosphate levels and acidocalcisome maintenance in *Trypanosoma brucei*. J. Biol. Chem. **285**:24131–24140.
47. **Madeira da Silva L, Beverley SM.** 2010. Expansion of the target of rapamycin (TOR) kinase family and function in Leishmania shows that TOR3 is required for acidocalcisome biogenesis and animal infectivity. Proc. Natl. Acad. Sci. U. S. A. **107**:11965–11970.
48. **Barquilla A, Saldivia M, Diaz R, Bart JM, Vidal I, Calvo E, Hall MN, Navarro M.** 2012. Third target of rapamycin complex negatively regulates development of quiescence in *Trypanosoma brucei*. Proc. Natl. Acad. Sci. U. S. A. **109**:14399–14404.
49. **Wirtz E, Leal S, Ochatt C, Cross G.** 1999. A tightly regulated inducible expression system for conditional gene knock-outs and dominant-negative genetics in *Trypanosoma brucei*. Mol. Biochem. Parasitol. **99**:89–101.
50. **Bellofatto V, Cross G.** 1989. Expression of a bacterial gene in a trypanosomatid protozoan. Science **244**:1167–1169.
51. **Hirumi H, Hirumi K.** 1989. Continuous cultivation of *Trypanosoma brucei* blood stream forms in a medium containing a low concentration of serum protein without feeder cell layers. J. Parasitol. **75**:985–989.
52. **Burkard G, Fragoso C, Roditi I.** 2007. Highly efficient stable transformation of bloodstream forms of *Trypanosoma brucei*. Mol. Biochem. Parasitol. **153**:220–223.
53. **Wickstead B, Ersfeld K, Gull K.** 2002. Targeting of a tetracycline-inducible expression system to the transcriptionally silent minichromosomes of *Trypanosoma brucei*. Mol. Biochem. Parasitol. **125**:211–216.
54. **Xong H, Vanhamme L, Chamekh M, Chimfwembe C, Van Den Abbeele J, Pays A, Van Meirvenne N, Hamers R, De Baetselier P, Pays E.** 1998. A VSG expression site-associated gene confers resistance to human serum in *Trypanosoma rhodesiense*. Cell **95**:839–846.
55. **Absalon S, Blisnick T, Bonhivers M, Kohl L, Cayet N, Toutirais G, Buisson J, Robinson D, Bastin P.** 2008. Flagellum elongation is required for correct structure, orientation and function of the flagellar pocket in *Trypanosoma brucei*. J. Cell Sci. **121**:3704–3716.
56. **Robinson D, Beattie P, Sherwin T, Gull K.** 1991. Microtubules, tubulin, and microtubule-associated proteins of trypanosomes. Methods Enzymol. **196**:285–299.
57. **Hill K, Hutchings N, Russell D, Donelson J.** 1999. A novel protein targeting domain directs proteins to the anterior cytoplasmic face of the flagellar pocket in African trypanosomes. J. Cell Sci. 112 Pt. **18**:3091–3101.
58. **Ralston KS, Hill KL.** 2006. Trypanin, a component of the flagellar Dynein regulatory complex, is essential in bloodstream form African trypanosomes. PLoS Pathog. **2**:e101. doi:10.1371/journal.ppat.0020101.
59. **Hannaert V, Albert MA, Rigden DJ, da Silva Giotto MT, Thiemann O, Garratt RC, Van Roy J, Opperdoes FR, Michels PA.** 2003. Kinetic characterization, structure modeling studies and crystallization of *Trypanosoma brucei* enolase. Eur. J. Biochem. **270**:3205–3213.
60. **Sherwin T, Schneider A, Sasse R, Seebeck T, Gull K.** 1987. Distinct localization and cell cycle dependence of COOH terminally tyrosinolated alpha-tubulin in the microtubules of *Trypanosoma brucei brucei*. J. Cell Biol. **104**:439–446.
61. **Kohl L, Sherwin T, Gull K.** 1999. Assembly of the paraflagellar rod and the flagellum attachment zone complex during the *Trypanosoma brucei* cell cycle. J. Eukaryot. Microbiol. **46**:105–109.
62. **Dilbeck V, Berberof M, Van Cauwenberge A, Alexandre H, Pays E.** 1999. Characterization of a coiled coil protein present in the basal body of *Trypanosoma brucei*. J. Cell Sci. **112**:4687–4694.
63. **Bonhivers M, Nowacki S, Landrein N, Robinson DR.** 2008. Biogenesis of the trypanosome endo-exocytotic organelle is cytoskeleton mediated. PLoS Biol. **6**:e105. doi:10.1371/journal.pbio.0060105.
64. **Nolan DP, Geuskens M, Pays E.** 1999. N-linked glycans containing linear poly-*N*-acetyllactosamine as sorting signals in endocytosis in *Trypanosoma brucei*. Curr. Biol. **9**:1169–1172.
65. **DeCenzo MT, Park ST, Jarrett BP, Aldape RA, Futer O, Murcko MA,**

**Livingston DJ.** 1996. FK506-binding protein mutational analysis: defining the active-site residue contributions to catalysis and the stability of ligand complexes. Protein Eng. **9**:173–180.
66. **Wear MA, Walkinshaw MD.** 2007. Determination of the rate constants for the FK506 binding protein/rapamycin interaction using surface plasmon resonance: an alternative sensor surface for $Ni^{2+}$-nitrilotriacetic acid immobilization of His-tagged proteins. Anal. Biochem. **371**:250–252.
67. **Sherwin T, Gull K.** 1989. The cell division cycle of *Trypanosoma brucei brucei*: timing of event markers and cytoskeletal modulations. Philos. Trans. R. Soc. Lond. B Biol. Sci. **323**:573–588.
68. **Rodríguez JA, Lopez MA, Thayer MC, Zhao Y, Oberholzer M, Chang DD, Kisalu NK, Penichet ML, Helguera G, Bruinsma R, Hill KL, Miao J.** 2009. Propulsion of African trypanosomes is driven by bihelical waves with alternating chirality separated by kinks. Proc. Natl. Acad. Sci. U. S. A. **106**:19322–19327.
69. **Absalon S, Kohl L, Branche C, Blisnick T, Toutirais G, Rusconi F, Cosson J, Bonhivers M, Robinson D, Bastin P.** 2007. Basal body positioning is controlled by flagellum formation in *Trypanosoma brucei*. PLoS One **2**:e437. doi:10.1371/journal.pone.0000437.
70. **Hutchings NR, Donelson JE, Hill KL.** 2002. Trypanin is a cytoskeletal linker protein and is required for cell motility in African trypanosomes. J. Cell Biol. **156**:867–877.
71. **Price HP, Peltan A, Stark M, Smith DF.** 2010. The small GTPase ARL2 is required for cytokinesis in *Trypanosoma brucei*. Mol. Biochem. Parasitol. **173**:123–131.
72. **Norville IH, Breitbach K, Eske-Pogodda K, Harmer NJ, Sarkar-Tyson M, Titball RW, Steinmetz I.** 2011. A novel FK-506-binding-like protein that lacks peptidyl-prolyl isomerase activity is involved in intracellular infection and in vivo virulence of *Burkholderia pseudomallei*. Microbiology **157**:2629–2638.
73. **Timerman AP, Wiederrecht G, Marcy A, Fleischer S.** 1995. Characterization of an exchange reaction between soluble FKBP-12 and the FKBP.ryanodine receptor complex: modulation by FKBP mutants deficient in peptidyl-prolyl isomerase activity. J. Biol. Chem. **270**:2451–2459.
74. **Lacomble S, Vaughan S, Gadelha C, Morphew M, Shaw M, McIntosh J, Gull K.** 2009. Three-dimensional cellular architecture of the flagellar pocket and associated cytoskeleton in trypanosomes revealed by electron microscope tomography. J. Cell Sci. **122**:1081–1090.
75. **Gadelha C, Rothery S, Morphew M, McIntosh JR, Severs NJ, Gull K.** 2009. Membrane domains and flagellar pocket boundaries are influenced by the cytoskeleton in African trypanosomes. Proc. Natl. Acad. Sci. U. S. A. **106**:17425–17430.
76. **Dolinski K, Muir S, Cardenas M, Heitman J.** 1997. All cyclophilins and FK506 binding proteins are, individually and collectively, dispensable for viability in *Saccharomyces cerevisiae*. Proc. Natl. Acad. Sci. U. S. A. **94**:13093–13098.
77. **Holwill ME, McGregor JL.** 1976. Effects of calcium on flagellar movement in the trypanosome *Crithidia oncopelti*. J. Exp. Biol. **65**:229–242.
78. **Ho HC, Suarez SS.** 2003. Characterization of the intracellular calcium store at the base of the sperm flagellum that regulates hyperactivated motility. Biol. Reprod. **68**:1590–1596.
79. **Woodward OM, Willows AO.** 2006. Nervous control of ciliary beating by $Cl^{-}$, $Ca^{2+}$ and calmodulin in *Tritonia diomedea*. J. Exp. Biol. **209**:2765–2773.
80. **Uppaluri S, Nagler J, Stellamanns E, Heddergott N, Herminghaus S, Engstler M, Pfohl T.** 2011. Impact of microscopic motility on the swimming behavior of parasites: straighter trypanosomes are more directional. PLoS Comput. Biol. **7**:e1002058. doi:10.1371/journal.pcbi.1002058.
81. **Broadhead R, Dawe HR, Farr H, Griffiths S, Hart SR, Portman N, Shaw MK, Ginger ML, Gaskell SJ, McKean PG, Gull K.** 2006. Flagellar motility is required for the viability of the bloodstream trypanosome. Nature **440**:224–227.
82. **Sherwin T, Gull K.** 1989. Visualization of detyrosination along single microtubules reveals novel mechanisms of assembly during cytoskeletal duplication in trypanosomes. Cell **57**:211–221.
83. **Briggs LJ, McKean PG, Baines A, Moreira-Leite F, Davidge J, Vaughan S, Gull K.** 2004. The flagella connector of *Trypanosoma brucei*: an unusual mobile transmembrane junction. J. Cell Sci. **117**:1641–1651.
84. **Moreira-Leite FF, Sherwin T, Kohl L, Gull K.** 2001. A trypanosome structure involved in transmitting cytoplasmic information during cell division. Science **294**:610–612.
85. **Robinson DR, Sherwin T, Ploubidou A, Byard EH, Gull K.** 1995. Microtubule polarity and dynamics in the control of organelle positioning, segregation, and cytokinesis in the trypanosome cell cycle. J. Cell Biol. **128**:1163–1172.
86. **Zhou Q, Liu B, Sun Y, He CY.** 2011. A coiled-coil- and C2-domain-containing protein is required for FAZ assembly and cell morphology in *Trypanosoma brucei*. J. Cell Sci. **124**:3848–3858.
87. **Sasse R, Gull K.** 1988. Tubulin posttranslational modifications and the construction of microtubular organelles in *Trypanosoma brucei*. J. Cell Sci. **90**:577–589.